

Neural Activity in Barrel Cortex Underlying Vibrissa-Based Object Localization in Mice

Daniel H. O'Connor,¹ Simon P. Peron,¹ Daniel Huber,¹ and Karel Svoboda^{1,*}

¹Janelia Farm Research Campus, Howard Hughes Medical Institute, 19700 Helix Drive, Ashburn, VA 20147, USA

*Correspondence: svobodak@janelia.hhmi.org

DOI 10.1016/j.neuron.2010.08.026

SUMMARY

Classical studies have related the spiking of selected neocortical neurons to behavior, but little is known about activity sampled from the entire neural population. We recorded from neurons selected independent of spiking, using cell-attached recordings and two-photon calcium imaging, in the barrel cortex of mice performing an object localization task. Spike rates varied across neurons, from silence to >60 Hz. Responses were diverse, with some neurons showing large increases in spike rate when whiskers contacted the object. Nearly half the neurons discriminated object location; a small fraction of neurons discriminated perfectly. More active neurons were more discriminative. Layer (L) 4 and L5 contained the highest fractions of discriminating neurons (~63% and 79%, respectively), but a few L2/3 neurons were also highly discriminating. Approximately 13,000 spikes per activated barrel column were available to mice for decision making. Coding of object location in the barrel cortex is therefore highly redundant.

INTRODUCTION

Information in the mammalian brain is represented by patterns of action potentials in neuronal populations (Adrian, 1932; Barlow, 1953; Hubel and Wiesel, 1962). One parameter describing neuronal populations is the fraction of neurons that are activated under particular behavioral conditions. A small fraction of active neurons is suggestive of sparse codes, which have high representational capacity and robustness (Olshausen and Field, 2004). A related parameter is the number of neurons carrying information about the sensory stimulus or particular phases of behavior (Shadlen and Newsome, 1994, 1998). Individual neurons in sensory cortex can discriminate stimuli comparable to behavioral performance of the entire animal (Britten et al., 1992; Celebrini and Newsome, 1994; Cohen and Newsome, 2009; Croner and Albright, 1999; Hernandez et al., 2000; Newsome et al., 1989; Palmer et al., 2007; Prince et al., 2000; Uka and DeAngelis, 2003; but see Cook and Maunsell, 2002). Redundancy in representations is a signature of fault tolerant coding. Understanding the patterns of activation across all members of a neuronal population, rather than specific subsets only, is

fundamental to deciphering the principles by which information is represented in the neocortex.

Common methods for measuring action potentials in the mammalian brain are not appropriate for sampling activity from all neurons in a population, including neurons that fire infrequently. Traditional extracellular recordings of action potentials (Hubel, 1957) have a selection bias for active neurons (Hromadka et al., 2008; Shoham et al., 2006); neurons that rarely spike go undetected. In addition, investigators often isolate single neurons for recording based on their responses to particular stimuli. More recent methods for recording multiple single neurons in parallel (Buzsaki, 2004) depend on large numbers of spikes to perform robust spike waveform clustering, again imposing a bias against neurons with low spike rates.

Methods for imaging neuronal populations *in vivo*, such as Ca²⁺ imaging, do account for all neurons in a recorded volume. However, cellular imaging is limited to superficial layers within the neocortex (Helmchen and Denk, 2005; Svoboda and Yasuda, 2006) and the available calcium sensors have so far not permitted reliable recording of individual action potentials (Sato et al., 2007; Tian et al., 2009). In addition, imaging with cellular resolution is rarely performed under conditions where the probed brain areas are known to be engaged in a behavior (Komiyama et al., 2010).

Intracellular and cell-attached recordings allow unambiguous detection of action potentials and do not suffer from activity-based selection biases. These methods have been applied in anesthetized (Brecht et al., 2003; de Kock et al., 2007; Helmchen et al., 1999; Manns et al., 2004; Moore and Nelson, 1998; Svoboda et al., 1997, 1999) and awake (Crochet and Petersen, 2006; de Kock and Sakmann, 2008, 2009; Gentet et al., 2010; Hromadka et al., 2008; Margrie et al., 2002; Poulet and Petersen, 2008) animals and generally have revealed low firing rates in sensory cortical areas. However, such recordings have not been reported under conditions where the probed neurons are required to drive a behavior. These methods also tend to report lower firing rates than traditional extracellular recordings (Brecht et al., 2003; Brecht and Sakmann, 2002; Margrie et al., 2002; Shoham et al., 2006). For these reasons, the activity of populations of sensory cortex neurons during performance of a sensory task is unknown.

The vibrissa representation area of the primary somatosensory cortex (barrel cortex) has favorable properties for relating sensory stimuli, neuronal responses, and behavior in the context of defined anatomical circuits (Diamond et al., 2008; Kleinfeld et al., 2006; O'Connor et al., 2009; Petersen, 2007). Each cortical layer corresponds neatly to distinct sets of excitatory neurons that participate in specific circuits (O'Connor et al., 2009; Petersen, 2007). Individual whiskers are mapped onto particular

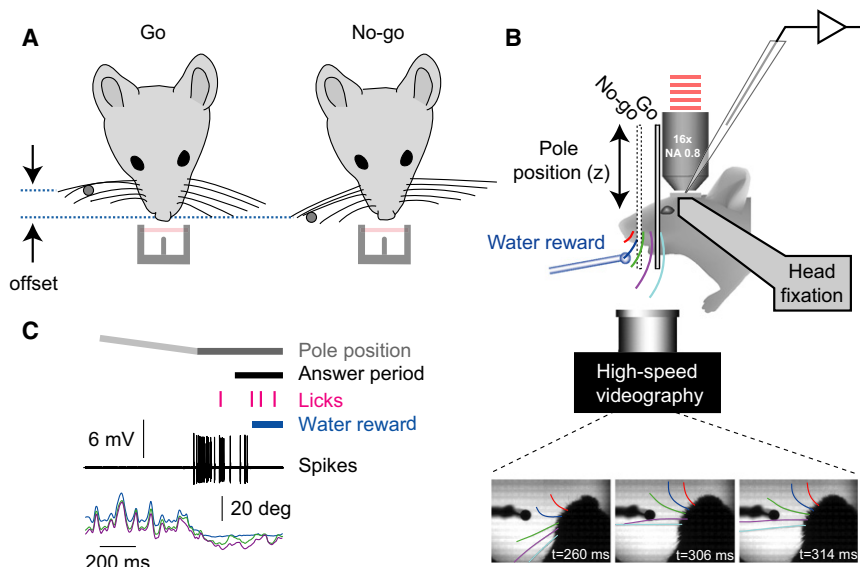


Figure 1. Cell-Attached Electrophysiology and Population Calcium Imaging during a Head-Fixed Object Localization Task

(A) Behavioral task. On each trial, a pole was presented to one side of the mouse face in either a “go” or a “no-go” position. The go and no-go positions were offset (by 4.29 mm) along the anterior-posterior axis. A “lickport,” comprising a water spout for reward delivery and an LED/phototransistor pair for recording licking, was placed in front of the mouse. The mouse had to use its whiskers to determine whether the pole was in the go or no-go position to either make (go) or withhold (no-go) a lick response.

(B) Schematic of apparatus. On each trial, the pole was moved vertically into reach of the whiskers, into either the go or the no-go location. High-speed video measured the positions and shapes of whiskers as they explored the pole (bottom image panels). Simultaneously, loose-seal, cell-attached recordings measured action potentials from single neurons in barrel cortex. Alternatively, two-photon microscopy measured activity-dependent fluorescence changes using a genetically encoded calcium indicator.

(C) Example go trial. Light gray slanted bar at top indicates that the pole is in motion; dark gray horizontal bar indicates that the pole is at the end of its range and in reach of the whiskers. The black horizontal bar indicates the start of an “answer period” in which the mouse must either make or withhold a lick response (see [Experimental Procedures](#)). The mouse made several licks (magenta ticks) and received a water reward (horizontal blue bar). The cell-attached recording (high-pass filtered) shows a burst of spikes that preceded the lick response of the mouse. Whisker position (bottom) reveals the motor program underlying object localization. See also [Figure S1](#).

“barrel” columns within the barrel cortex (Simons, 1978; Welker, 1971; Woolsey and Van der Loos, 1970). Several studies have described the responses of individual cortical neurons to passive whisker deflections in anesthetized animals (Armstrong-James et al., 1992; Brecht et al., 2003; de Kock et al., 2007; de Kock and Sakmann, 2008; Manns et al., 2004; Moore and Nelson, 1998; Simons, 1978). A smaller number of studies have examined single-unit (Curtis and Kleinfeld, 2009; Jadhav et al., 2009; Vijayan et al., 2010) or multiunit (Simons et al., 1992) responses in barrel cortex of behaving animals. Very few studies have measured activity in animals performing choice-based somatosensory tasks in which a correct response depends on the value of a stimulus so that animals must attend to the stimuli (Krupa et al., 2004; Pantoja et al., 2007; von Heimendahl et al., 2007). Neuronal activity during such task-driven somatosensation can differ dramatically from passive stimulation (Krupa et al., 2004). Here, we used loose seal cell-attached recordings and two-photon imaging to measure barrel cortex activity in a recently developed head-fixed object localization task (O’Connor et al., 2010).

RESULTS

We trained head-fixed mice to perform a whisker-based barrel cortex-dependent object localization task. Mice used their whiskers to determine the location of a small pole presented to one side of the head, and reported with go/no-go licking whether the pole was in a target (go) or a distracter (no-go) position (Figure 1). Mice had all but a single row of their whiskers trimmed to lengths too short to reach the pole. Three spared

whiskers (D2-D4 and C1-C3 for the electrophysiological and imaging experiments, respectively) routinely contacted the pole and could thus provide information to the mouse about the pole location. For each trial we acquired high-speed video of the whiskers. We made loose-seal cell-attached recordings (Hromadka et al., 2008; [Figure S1](#) available online) targeted to relevant whisker barrel columns using intrinsic signal imaging. This recording method selects neurons independent of action potential activity and permits accurate sampling of the spike trains produced by a population of neurons (de Kock et al., 2007; de Kock and Sakmann, 2008; Hromadka et al., 2008). Here, we applied this method to barrel cortex of animals performing tactile localization. We recorded from neurons in all cortical layers. Mice performed hundreds of trials in individual sessions ([Figure S1E](#)) while we recorded action potentials from single neurons. In separate experiments, we used two-photon calcium imaging (Svoboda and Yasuda, 2006) to monitor populations of layer 2/3 neurons during performance of the tactile localization task.

Barrel Cortex Neurons Show Diverse Response Types and Large Modulation of Activity

We sampled from all neurons encountered by our recording pipette (see [Supplemental Experimental Procedures](#)). Responses differed dramatically among neurons ([Figure 2](#)), even within individual electrode penetrations ([Figure S2A](#)). A few neurons had high firing rates (up to ~60 Hz), while other neurons did not spike ([Figures 2](#) and [S2B](#)). Mice typically began whisker movement shortly before the stimulus pole was within reach of the whiskers (O’Connor et al., 2010; [Figure 1C](#)). Peristimulus

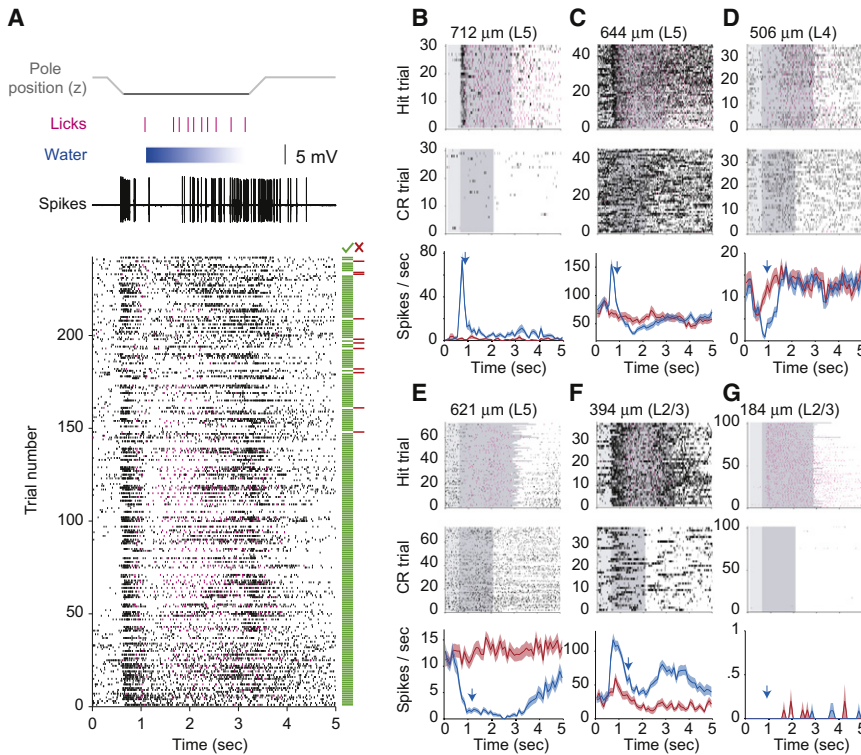


Figure 2. Diverse Response Types and Large Spike Rate Modulations in Barrel Cortex during Object Localization

(A) Example go trial (top) showing behavior and action potentials. A raster plot (bottom) for 242 trials (go and no-go randomly interleaved) for the same neuron (L5, 730 μ m) showing action potential times (black ticks) and licks (magenta ticks). Horizontal green and red bars at the right of each raster indicate trials that were correct (green check) and incorrect (red cross), respectively.

(B–G) Raster plots (top) and peristimulus time histograms (PSTHs; bottom) during object localization. Trials are separated into hits (top) and correct rejections (middle). Light gray shading on the raster indicates that the pole is in motion; dark gray shading indicates that the pole is at the end of its range and within reach of the whiskers. Black ticks, spikes. Magenta ticks, licks. PSTHs aligned to the start of the trial (bottom) show firing rates for hit (blue) and correct rejection (red) trials (error shading \pm SEM). The blue arrow indicates the mean reaction time of the mouse during the recording. Raster plots show equal numbers of hit and correct rejection trials; the PSTHs include all trials of each type. (B and C) Neurons with phasic increases in spike rate when the pole becomes available on go trials. (D and E) Neurons with decreases in spike rate when the pole becomes available on go trials. (F) Neuron with a multimodal response. (G) Neuron that spikes extremely rarely during the task, and never before the mean reaction time of the mouse.

See also Figure S2.

time histograms (PSTHs) aligned to the start of the trial often showed robust modulations in firing rate over the course of the trial (Figures 2 and S2). This is because the first whisker-object contact occurred reproducibly to within 100 ms (PSTH bin size 50 ms). As the pole moved into reach of the whiskers, mice whisked over the target location, causing strong whisker-object contact on go trials (O'Connor et al., 2010). Mice largely avoided the distracter location, implying that on no-go trials contacts were sparser and weaker. This active sensing strategy thus resulted in strong forces on the whiskers on go trials, and weaker forces, or even no contact, on no-go trials. A common motif in the pattern of neural activity therefore involved a phasic increase in spike rate on go trials, but not on no-go trials (Figures 2B and 2C). Other modulations in firing rate comprised: tonic increases in rate (Figures 2F and S2C), tonic decreases in rate (Figures 2D and 2E; see also Curtis and Kleinfeld, 2009; Jadhav et al., 2009; Krupa et al., 2004) or multimodal responses (Figure 2F; Krupa et al., 2004; Pantoja et al., 2007). We also encountered neurons with more complex firing patterns, such as responding bimodally with first a decrease and then an increase in rate, elevated firing rates during the intertrial interval, or responding mainly while the mouse consumed rewards (Figure S2C). Most modulated neurons appeared to differentiate trial type. Many neurons showed significant changes in spike rate during episodes of free whisking in air (not against the pole) compared with periods of nonwhisking, in a layer-specific manner (Figure S3A; see also de Kock et al., 2007).

A Small Fraction of Neurons Fires the Vast Majority of Spikes

We quantified the firing rates of barrel cortex neurons across cortical layers (Figure 3). We first report the overall firing rates, averaged across all trial epochs (f_{overall}). Averaged across layers the firing rate was $f_{\text{overall}} = 7.4$ Hz (Table 1; $N = 106$ neurons, including $N = 14$ “silent neurons” whose spontaneous firing rates have an upper bound of <0.0083 Hz and were found predominantly in L2/3 and L6; purple symbols in Figure 3A; see Experimental Procedures). Forty-four percent of neurons had $f_{\text{overall}} < 1$ Hz. However, the distribution of firing rates featured a long tail caused by a small fraction of highly active neurons. Eleven percent had $f_{\text{overall}} > 20$ Hz.

Median firing rates for each layer, including silent neurons, were (in Hz): L2/3, 0.18; L4, 3.48; L5, 9.13; L6, 0.48 (Table 1). The firing rates differed significantly across layers, with L2/3 and L6 showing lower rates than L4 and L5 (Figure 3C; one-tailed K-S test on L2/3/L6 versus L4/L5, $p < 0.001$).

The least active half of the neurons contributed less than 3% of the spikes (Figure 3D). Conversely, a small fraction of neurons fired the vast majority of spikes, with the most active 10% of neurons contributing $\sim 50\%$ of the spikes (Figure 3D; see also Hromadka et al., 2008).

Similar results were found when analyzing spike rates across different epochs of the behavioral task, including the intertrial interval. A small fraction of neurons always produced the vast majority of spikes (Figure S3B). For individual neurons, spike

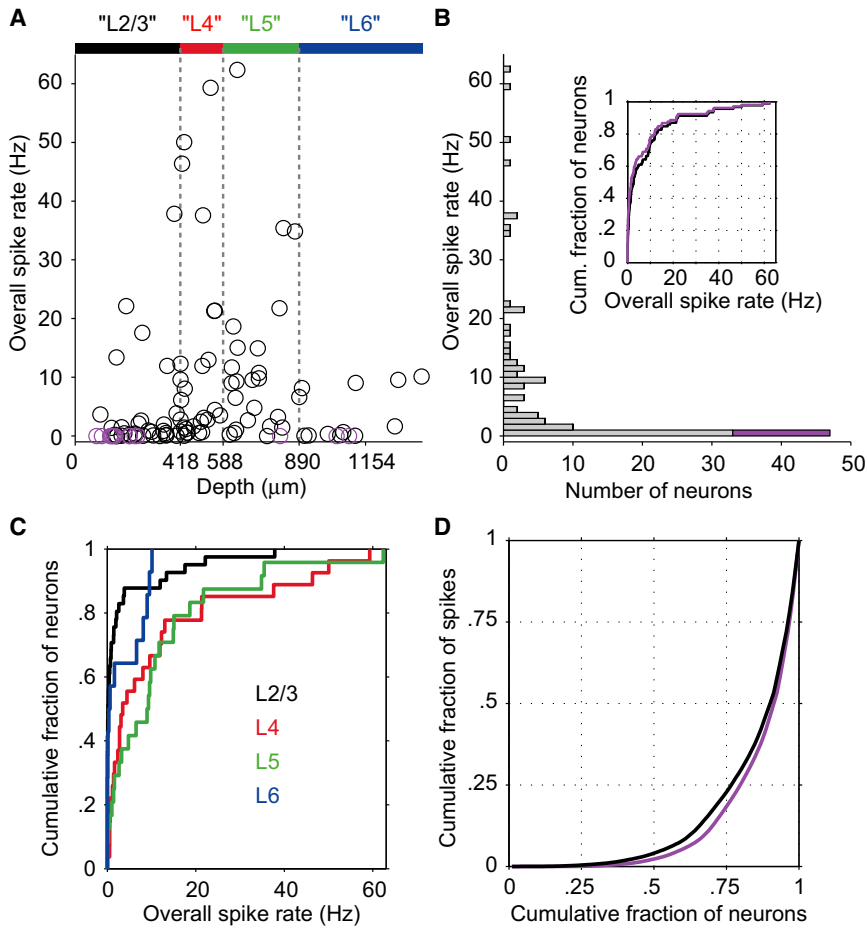


Figure 3. Most Spikes Are Fired by a Small Minority of Neurons

(A) Firing rate for each neuron during task performance (averaged across all behavioral epochs), as a function of cortical depth. Each circle corresponds to a single neuron (purple, "silent neurons") (see [Experimental Procedures](#)). Laminal boundaries are indicated by colored bars at top and by vertical dashed lines.

(B) Histogram of the firing rate data in (A). Purple bar indicates number of "silent neurons." Inset, cumulative histogram of the same data, both omitting (black) and including (purple) the silent neurons.

(C) Cumulative histogram of overall firing rate data from (A), by cortical layer. Includes "silent neurons."

(D) Plotting cumulative fraction of neurons against cumulative fraction of total spikes (black, omitting silent neurons; purple, including silent neurons) shows that most spikes come from a minority of neurons.

See also [Figure S3](#).

The large range of spike rates observed in cortical neurons ([Figure 3](#)) creates challenges for calcium imaging. At one extreme, the limited sensitivity of current methods precludes detecting activity in neurons showing very low activity (<3 action potentials in 0.5 s); only robust bursts of activity are therefore detected ([Tian et al., 2009](#)). At the other extreme, indicator saturation may obscure firing rate modulation in neurons with the highest firing rates. Rates of fluorescence

transients are therefore expected to be much lower than spike rates. Simulations of fluorescence data based on electrophysiology spike times are consistent with this view ([Figure S4](#)).

Highly Active Neurons Are Sparsely Distributed in L2/3

Cell-attached recordings have some drawbacks. Only one neuron is interrogated at a time, and the cell type and location, with respect to other neurons, are not well defined. To overcome these limitations, we performed *in vivo* calcium imaging of population activity in L2/3 ([Andermann et al., 2010](#); [Greenberg et al., 2008](#); [Kerr et al., 2007](#); [Komiyama et al., 2010](#); [Sato et al., 2007](#); [Stosiek et al., 2003](#)) during the tactile localization task.

We delivered the genetically encoded indicator GCaMP3 ([Tian et al., 2009](#)) to barrel cortex via infection with adenoassociated virus (AAV2/1, *synapsin-1* promoter). The behavioral apparatus was mounted under a custom microscope. Continuous two-photon calcium imaging (frame rate, 4 Hz) was performed through an implanted imaging window. Regions of interest corresponding to individual neurons (108–177 neurons per animal) were defined in a semiautomated manner. Fluorescence transients, corresponding to small bursts of action potentials (>3; [Tian et al., 2009](#)), were detected automatically (see [Supplemental Experimental Procedures](#)).

A sparse subset of L2/3 neurons showed robust fluorescence transients ("events") of up to ~220% $\Delta F/F$ ([Figure 4A](#)) (event rates, 0–0.12 Hz) with rapid kinetics (decay time, $t_{1/2}$, 543 ± 462 ms; median \pm interquartile range (IQR); [Figure S4F](#)). High event rates were seen in only a small subset of neurons, with the majority showing low, near zero, event rates ([Figures 4B and 4C](#)). Active neurons were apparently randomly distributed within L2/3. Retrospective histological analysis revealed that most of the neurons showing robust fluorescence changes were not GABAergic (not shown). The imaging experiments therefore confirm that a sparse subset of neurons produces most of the activity in L2/3.

What Barrel Cortex Neurons Tell the Mouse about Object Location

What Barrel Cortex Neurons Tell the Mouse about Object Location

To determine the pole location, mice whisked against the pole, inducing contact forces and moments, which in turn caused spikes in barrel cortex neurons ([Figure 5](#)). In addition to being a source of feedback control for further whisking ([Mitchinson et al., 2007](#); [O'Connor et al., 2010](#)), spikes in the barrel cortex provided a basis for the mouse's decision. In the remainder of

Table 1. Firing Rates of Barrel Cortex Neurons during Active Somatosensation

Layer	Including "Silent Neurons"			Excluding "Silent Neurons"		
	Mean ± SD	Median ± IQR	N	Mean ± SD	Median ± IQR	N
L2/3	3.04 ± 7.36	0.18 ± 1.58	41	4.16 ± 8.33	0.62 ± 2.51	30
L4	11.96 ± 16.50	3.48 ± 11.57	27	11.96 ± 16.50	3.48 ± 11.57	27
L5	11.87 ± 14.34	9.13 ± 13.47	24	12.39 ± 14.43	9.29 ± 13.14	23
L6	2.30 ± 4.09	0.48 ± 8.11	14	3.85 ± 4.17	1.12 ± 8.45	12
All	7.35 ± 12.59	1.54 ± 9.45	106	8.47 ± 13.16	2.63 ± 9.93	92

SD, sample standard deviation; IQR, interquartile range.

this paper, we explore what information individual barrel cortex neurons might provide about object location. First, we estimate the neural signals in the barrel cortex that could contribute to the mouse's sensory-motor decision. Next, we directly ask what fraction of barrel cortex neurons discriminates between trial types, and how well individual neurons do so. We find that, despite the many relatively silent neurons in barrel cortex, a large fraction of neurons distinguishes between go and no-go trials.

The Number of Spikes Evoked on Different Trial Types during Object Localization

As the pole moved into the whisker field, mice explored the vicinity of the target location, and largely avoided the distracter location (O'Connor et al., 2010). On go trials, whiskers contacted the pole, often multiple times (up to ten), and underwent large-amplitude bending before the reaction time (Figures 5 and 6A). The spiking response of individual neurons in barrel cortex therefore reflects multiple whisker-pole contacts, usually on multiple whiskers, as well as progressive increases in whisker bending (Figure 6A), which causes lateral and axial stresses in the follicle (Birdwell et al., 2007). In contrast, when the pole was in the distracter position, contact between whiskers and the pole was much less frequent and weaker (not shown). The mouse's motor strategy therefore produced different temporal patterns of forces on the whiskers on different trial types.

We measured the number of spikes evoked (i.e., number of spikes minus the number of spikes expected from the baseline firing rate) prior to the mean reaction time (Figure 6B) for hit and correct rejection trials. Most neurons showed increases in spike rate (the "evoked" number of spikes can be negative; Figure 6B), with a mean (±SD) number of evoked spikes of 2.4 ± 7.5 (median ± IQR: 0 ± 1.7) on hit trials and -0.04 ± 1.7 (median ± IQR: 0 ± 0.36) on correct rejection trials (Figures 6B and 6C). These distributions differed among cortical layers (Figures 6B and 6C), with L4 and L5 neurons showing a larger number of evoked spikes compared to L2/3 and L6 neurons (one-tailed K-S test on L4/L5 versus L2/3/L6, $p = 0.008$). Thirty four percent of all neurons showed significant (positive or negative) evoked spikes on hit trials (Figure 6D, left; permutation test; see Supplemental Experimental Procedures). In contrast, few neurons showed significant evoked spikes on correct rejection trials (4%; Figure 6D, right).

The mouse presumably bases its decision on differences in spiking during go and no-go trials. The distribution of mean spike count difference between hits and correct rejections had a median of zero spikes (Figure 7A). Treating increases and decreases in spike count difference as equivalent (by taking the absolute value of the spike count difference distribution), the median was 0.72 spikes (Figure 7A). Spike count differences between trial types were higher for L4 and L5 neurons than for

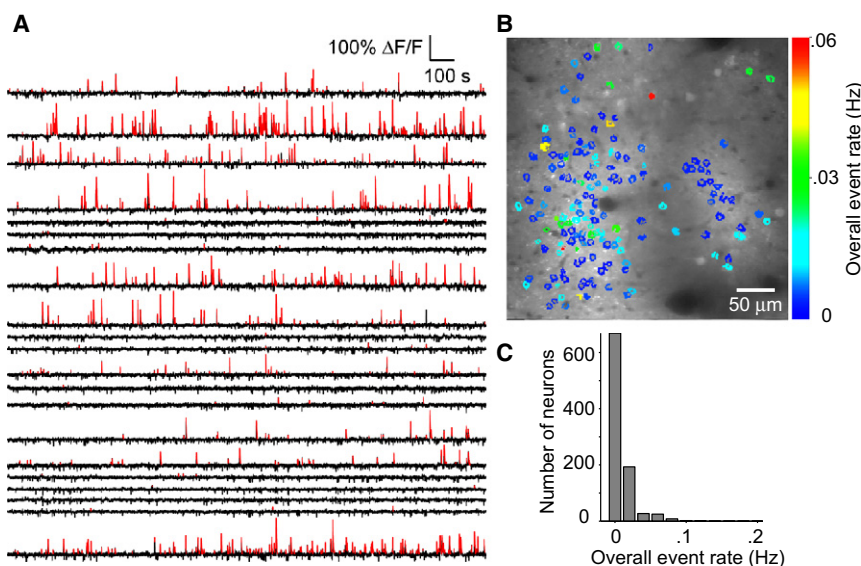


Figure 4. Neurons with High Event Rates Are Sparse in L2/3

(A) Fluorescence ($\Delta F/F$) time series recorded simultaneously from 21 L2/3 neurons in a mouse performing the tactile localization task. Transient increases in fluorescence ("events") are shown in red.

(B) Pixel regions of interest corresponding to different neurons are shown colored by overall event rate (across all behavioral epochs and trial types for one behavioral session) and are superimposed on a mean z-projection two-photon image from a single behavioral trial. Same session as in (A).

(C) Histogram of event rates across seven behavioral sessions from four mice. Most neurons fall into the lowest event rate bin, but there is a long tail of more active neurons. For three mice, neurons were measured in two sessions and appear twice in the histogram; there are 551 unique neurons. See also Figure S4.

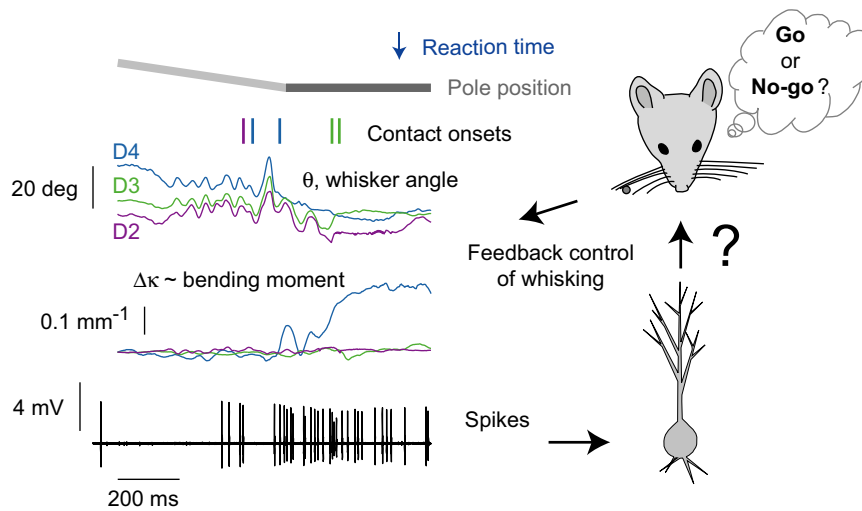


Figure 5. What Do Individual Barrel Cortex Neurons Tell the Mouse about Object Localization?

Events from an example hit trial, and schematic of mouse's task. As the pole comes into reach of the whiskers, the mouse whisks, makes multiple whisker-pole contacts, and experiences progressive whisker bending (and changing moment at the follicle). These events are associated with spiking of the barrel cortex neuron; 730 μm (L5). The mouse presumably monitors the population of barrel cortex neurons to decide whether to make a go or no-go response. We performed analyses to address the question of how much information individual barrel cortex neurons provide about the correct behavioral response. Light gray slanted bar at top indicates that the pole is in motion; dark gray horizontal bar indicates that the pole is at the end of its range. Electrophysiology trace (high-pass filtered voltage) shows action potentials from the recorded neuron (principal whisker: D4). Whisker angle (θ) and change in curvature ($\Delta\kappa$) are shown for whiskers D4 (blue), D3 (green), and D2 (purple). Contact times (onset times only) are shown by the colored tick marks above the whisker position traces.

L2/3 and L6 neurons (Figure 7A; one-tailed K-S test on L4/L5 versus L2/3/L6, $p < 0.001$). Overall, 35% of neurons showed a significant difference in spike count between hit and correct rejection trials (Figure 7B).

The distribution of differences in mean spike count between hits and correct rejections (Figures 7A and 7B) shows that a small minority of neurons provides the majority of the total spike count difference (Figure 7C). Fifty percent of the differential spikes were provided by only 8% of the neurons (Figure 7C).

We used published values for the number of neurons in a barrel column (L1/L2/3: 1947; L4: 1796; L5: 1316; L6: 1415; Lefort et al., 2009; our estimates will change according to the cell counts used; cf. Tsai et al., 2009) to estimate the total difference in spike count overall between hits and correct rejections for a barrel column, prior to the mean reaction time (Figure S5). L4 and L5 showed the largest differences in spike count (Figure S5B; differences of 7141 ± 2896 and 5395 ± 2176 spikes/trial). L6 showed a small difference (782 ± 662 spikes/trial). The L2/3 spike count difference was 407 ± 673 spikes/trial (one outlier near the L2/3 \rightarrow L4 border, apparent in histograms of Figures 6B, 6C, and 7A, was excluded). Thus, the total difference in spike count between hits and correct rejections for one barrel column was $13,725 \pm 3743$ spikes/trial.

Because the mice routinely made whisker-pole contact with up to three whiskers (D2-4), as many as 41,000 differential spikes (hits minus correct rejections) in barrel cortex were available to mice in making their sensory-motor decision. This number does not account for activity in barrel columns corresponding to cut whiskers, which may also contribute spikes relevant to the sensory-motor decision, especially in mice that have experienced prolonged whisker trimming (Fox, 2002).

The differences among layers in evoked activity (Figure 6) paralleled differences in baseline activity (Figure S3B; "intertrial interval" shows baseline activity), with L2/3 and L6 showing in both cases less activity than L4 and L5.

A Large Fraction of Neurons Discriminate Trial Types

We used detection analysis (Green and Swets, 1966) to determine how well individual neurons distinguished between hit and correct rejection trials (Figures 8, S6, and S7; see Experimental Procedures). Because the temporal profile of firing rates carries stimulus information, we used a PSTH-based classification scheme rather than one based on spike count alone (see Experimental Procedures). We focused on correct trials (i.e., hits and correct rejections) because we could not be certain that on error trials the whisking, and hence the neural activity, was related to the object localization task (including both correct and incorrect trials gave similar results; Figure S7A). Activity up to the reaction time was considered. Overall, the firing of $43\% \pm 3\%$ of neurons (including "silent neurons") discriminated between trial types (Figure 8A). Individual neurons could discriminate either by increases or decreases in firing rate (Figure 2) or both (Figure S2C). Several individual neurons discriminated nearly perfectly (up to 99.6% of trials categorized correctly, Figure 8A), better than the mouse (Figure S7A). Other neurons showed no discrimination (Figure 8A; data points below the horizontal gray lines). Including spikes recorded across the entire trial (rather than only the period before the reaction time) led to a higher fraction of neurons that discriminate, $59\% \pm 3\%$ (not shown), but this includes the contribution of activity related to reward and other factors.

The fraction of neurons discriminating above chance differed among cortical layers (Figure 8B), with L4 and L5 containing higher fractions than L2/3 and L6 (one-tailed bootstrap test of difference between L4/L5 and L2/3/L6, $p < 0.001$). However, a few individual neurons in L2/3 were highly discriminative (Figure 8B; up to 92% correct), indicating that coding of object location is sparse for L2/3 neurons.

Using published values for the number of neurons in each layer of a barrel column (Lefort et al., 2009), we estimate that $\sim 43\%$ of all neurons in a barrel column discriminate trial types in our task.

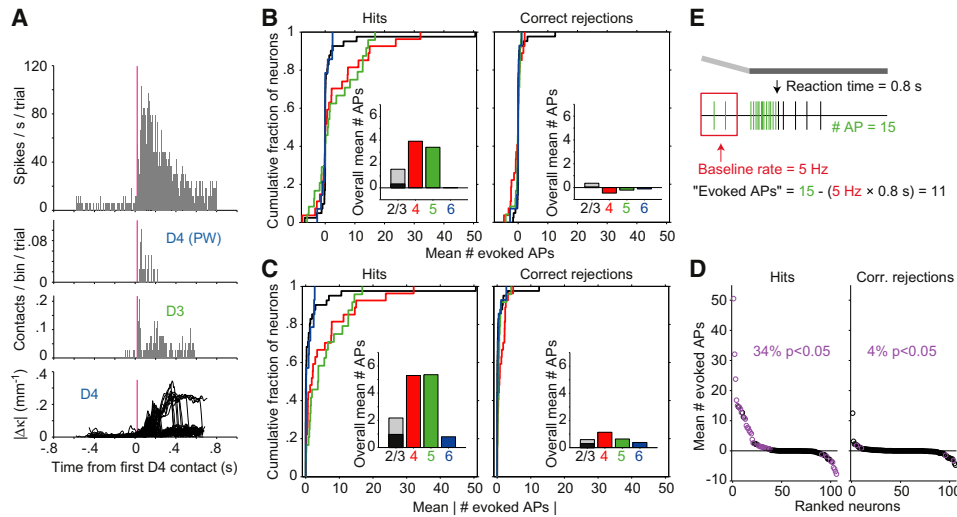


Figure 6. The Number of Spikes Evoked on Different Trial Types during Object Localization

(A) Histograms (40 hit trials; 5 ms bins) of spike count (top) and whisker-pole contact times for D4 and D3 (middle), and rectified change in D4 whisker curvature ($\Delta\kappa$), all aligned to time of the first D4 whisker-pole contact (time 0). Neuron same as in Figure 5. PW, principal whisker. Vertical magenta lines (20 ms) show the approximate time of increased spike rate.

(B) Distributions for each layer of the number of spikes (“APs”) evoked above baseline (calculation illustrated in E) prior to the mean reaction time for hits (left) and correct rejections (right). Insets, the mean of the distribution for each layer. Most evoked spikes occur on hit trials and are due mainly to L4 and L5 neurons. For L2/3, insets show mean both excluding (black) and including (gray) an outlier neuron located near the L2/3→L4 border (see Results).

(C) Similar to (B) but showing the distributions of the absolute value of the number of evoked spikes; the “evoked” number of spikes can be negative. This shows the total number of differential spikes for hits (left) and correct rejections (right). Insets, the mean of the distribution for each layer.

(D) Same data as in (B) for hits (left) and correct rejections (right), with neurons ranked by the number of evoked spikes along the x axis. Neurons showing a statistically significant number of spikes evoked above baseline are indicated by purple symbols. Note that this analysis ignores the temporal pattern of spike rate changes; bimodal rate modulations that average to the baseline rate will not be significant. Thirty-four percent of neurons show a significant number of evoked spikes on hit trials. On correct rejection trials, the fraction (4%) is not different from the expected false-positive rate ($\alpha = 0.05$).

(E) Schematic of computation of “evoked APs.” The number of action potentials expected (due to the baseline firing rate) prior to the mean reaction time was subtracted from the actual number of action potentials (shown in green) prior to the mean reaction time. See Supplemental Experimental Procedures for details. In (B–D), all panels include only spikes prior to the mean reaction time and include “silent neurons.”

See also Figure S5.

The overall spike rate of a neuron was a strong predictor of its discrimination ability (Figures 8C and 8D). All neurons with rates >10 Hz discriminated trial types (Figures 8C and 8D), whereas no neurons with overall rates <0.49 Hz discriminated. Neurons with rates of 0.5–10 Hz showed large heterogeneity in discrimination ability, ranging from nearly perfect to chance-level (Figure 8C). The greater discrimination ability of high firing-rate neurons could be because (1) more active neurons have greater statistical power due simply to having more spikes; or (2) the more active neurons are more discriminative even on a per-spike basis, perhaps because they are connected into the network in a privileged manner. However, neurons with similar spike rates could vary widely in discrimination ability, suggesting that having more spikes per se does not fully explain the superior discrimination performance of highly active neurons.

We examined single-neuron performance as a function of time within the trial (Figure 8E). The time course of single-neuron performance was heterogeneous (Figure 8B), with some neurons achieving almost perfect discrimination nearly as soon as the pole came into reach of the whiskers, and other neurons showing a gradual increase in performance or not at all. Single-neuron performance closely paralleled changes in whisker curvature (Figure 8B), which corresponds to mechanical stresses at the

whisker follicle (Birdwell et al., 2007). On average, neurons in L4 and L5 showed the fastest increases in single-neuron performance and the highest overall performance levels (Figure 8E).

Discriminative Neurons Are Sparse in L2/3 and Include Excitatory Neurons

A sparse subset of individual L2/3 neurons was highly discriminative in calcium imaging experiments. These neurons showed an increased number of fluorescence transients during either hit or correct rejection trials (Figures 9 and S8). Retrospective immunohistochemistry (Figure S9) revealed that the discriminative neurons were not GABAergic (Figures 9 and S8) and were therefore presumably excitatory.

DISCUSSION

Quantitative sensory decision-making paradigms in primates have been critical to reveal the relationship between neuronal activity in the neocortex and behavioral choice (Newsome et al., 1989; Romo et al., 1998). Here, we have extended this approach to head-fixed mice performing an active tactile object localization task (O’Connor et al., 2010), to study the neural basis of vibrissa-based somatosensation. We used an in vivo

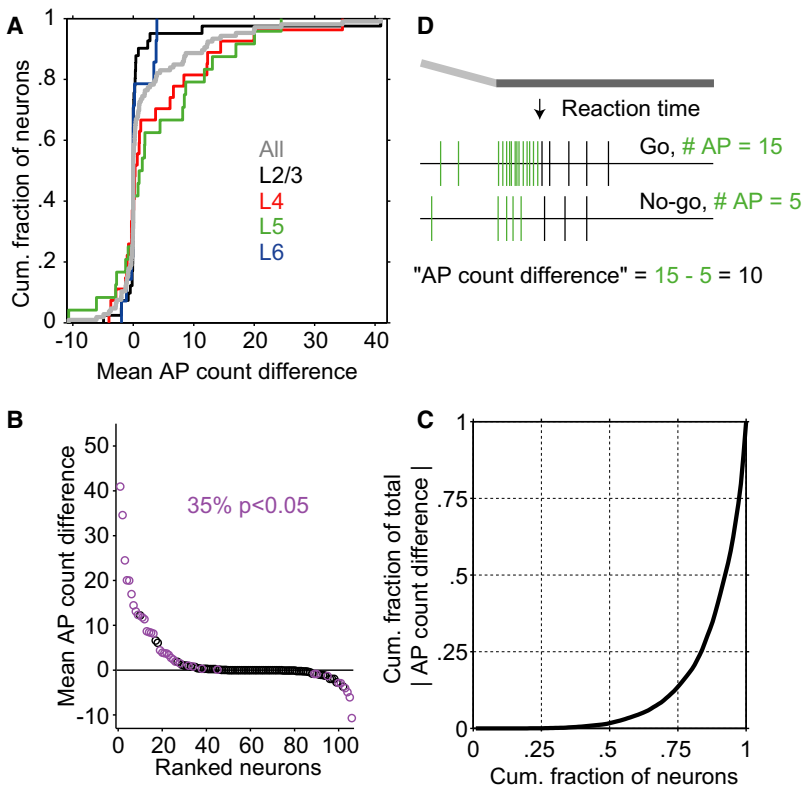


Figure 7. The Spike Count Difference between Hit and Correct Rejection Trials

(A) Distribution of the mean spike count on hit trials minus the mean spike count on correct rejection trials, i.e., of the differential spikes between trial types (computation illustrated in D). The full data set ("All") is shown in gray; individual layers are distinguished by color. The median of the distribution is zero spikes. Treating increases and decreases in spike count as equally relevant by taking the distribution of absolute value differences gives a median of 0.72 spikes; i.e., the median number of differential spikes for hits and correct rejections is $\sim 3/4$ spike per trial per neuron.

(B) Same data as in (A), with neurons ranked by the difference in spike count between hits and correct rejections. Thirty-five percent of neurons show a significant difference in the spike count between hits and correct rejections. Twenty-eight of one-hundred and six neurons showed significantly higher spike counts on hit trials compared with correct rejection trials (purple points above the line at 0). Nine of one-hundred and six showed significantly lower spike counts on hits compared with correct rejections (purple points below zero).

(C) Plotting cumulative fraction of neurons against cumulative fraction of the total rectified spike count difference between hits and correct rejections shows that most differential spikes come from a small fraction of neurons.

(D) Schematic of computation of "AP count difference." The number of spikes prior to the mean reaction time (measured for go-trials only; spikes before reaction time shown in green) on no-go trials was subtracted from the number of spikes prior to the mean reaction time on go trials. See [Supplemental Experimental Procedures](#) for details.

In (A–C), all panels include only spikes prior to the mean reaction time and include "silent neurons."

See also [Figure S5](#).

electrophysiology recording method (de Kock et al., 2007; de Kock and Sakmann, 2008; DeWeese et al., 2003; Hromadka et al., 2008; Margrie et al., 2002) that does not select for neurons based on firing rate and that does not affect the intracellular composition of the recorded cells as does whole-cell recording (Margrie et al., 2002). Action potential rates of most neurons were far lower than those often reported from sensory cortex of animals performing sensory choice-based tasks (Shadlen and Newsome, 1994, 1998). This likely reflects the fact that neurons recorded in such studies are typically isolated based on robust spiking, often in response to particular stimuli. This leads to a sampling bias that has long been appreciated (Mountcastle, 1995; Wurtz, 1968). The most active 10% of neurons contributed the majority of spikes. A small subset of neurons showed overall spike rates that could exceed 50 Hz. These highly active neurons have been reported in the barrel cortex of behaving rats (Curtis and Kleinfeld, 2009; Jadhav et al., 2009; Krupa et al., 2004; Pantoja et al., 2007; Vijayan et al., 2010; with Curtis and Kleinfeld, 2009; Jadhav et al., 2009; Vijayan et al., 2010 showing a >10 -fold spread of overall action potential rates). Both overall (Otazu et al., 2009) and stimulus-specific activity levels (Hubel et al., 1959; Moran and Desimone, 1985) are known to be regulated by the attentional or motivational state of the animal. Possible differences in the spike rates recorded in

ours and other studies (Crochet and Petersen, 2006; de Kock and Sakmann, 2008, 2009; Margrie et al., 2002; Poulet and Petersen, 2008) likely reflect behavioral state (see also Vijayan et al., 2010).

The electrophysiological recording method used in this study, loose-seal cell-attached patch-clamping, does not select on the basis of neuronal activity, but recordings are established based on the ability of the pipette and a cell to come into contact such that the electrical resistance across the pipette tip is increased. Large cells may therefore be recorded with a higher probability than small cells, as their greater surface area presumably makes contact between pipette and cellular membrane more likely.

In our electrophysiological experiments in trained mice, it was necessary to record from multiple neurons across multiple days; we therefore were unable to routinely label recorded neurons. Estimates of recording depth were instead based on micromanipulator readings and parallel calibrations based on histology. The expected error in localizing the pipette ($\pm 30 \mu\text{m}$, see [Supplemental Experimental Procedures](#)) is expected to smear the boundary between layers, with disproportionately larger effects on the thinner layers. In addition, in a small fraction of cases we may have recorded from dendrites of neurons and thereby misassigned the neuron's layer. In our two-photon imaging experiments, laminar location was unambiguous.

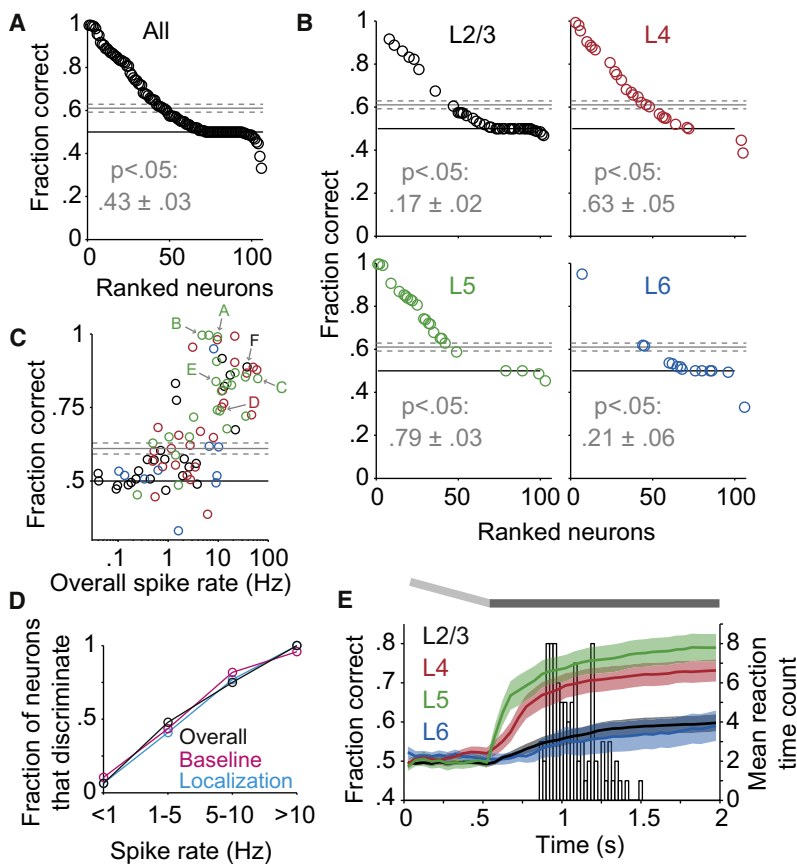


Figure 8. A Large Fraction of Single Neurons Discriminate between Trial Types

(A) Fraction of trials discriminated correctly (hits versus correct rejections) for each individual neuron. Fraction correct is determined as the area under the receiver-operating characteristic (ROC) curve for a classifier based on PSTH shape, using only spikes up to the mean reaction time of the mouse (see [Experimental Procedures](#)). Neurons are ranked by performance from best to worst along the x axis. The horizontal solid gray line shows the mean 95th percentile from trial label-shuffled data (\pm SEM, dashed lines; see [Supplemental Experimental Procedures](#)). Data points below this line show neurons that do not discriminate above chance level. The gray text indicates that 43% \pm 3% of the neurons discriminate above chance. The best neuron discriminates at 99.6% correct.

(B) Same as (A), but with neurons from each cortical layer shown separately. The ranking of the neurons along the x axis is preserved from (A).

(C) Fraction of trials discriminated correctly versus overall spike rate for each individual neuron. Cortical layers are distinguished by color (same as B). Neurons with overall spike rates < 0.03 Hz (all with fraction correct = 0.5) are not shown. Neurons shown in [Figure 2](#) panel letters (panel G neuron has spike rate < 0.03 Hz and is not shown).

(D) Fraction of neurons in different spike rate bins that discriminate significantly. Different colors show spike rate measured across all behavioral epochs (“Overall”), during the trial baseline period (before the pole is in reach of the whiskers; “Baseline”), or during the period in which the mouse makes whisker-pole contact (“Localization”).

(E) Fraction correct as a function of time from start of the trial (see [Experimental Procedures](#)), measured for indi-

vidual neurons but averaged across each cortical layer. Error shading shows SEM. On average, neurons in L4 and L5 discriminate rapidly and at a high level, whereas neurons in L2/3 and L6 discriminate less rapidly and at a lower level. Light gray slanted bar at top indicates that the pole is in motion; dark gray horizontal bar indicates that the pole is at the end of its range and in reach of the whiskers. The histogram in the background shows the mean reaction time of the mouse during each recording.

In all panels, plots include 92 neurons plus 14 “silent neurons.” See also [Figures S6 and S7](#).

We often observed robust stimulus-evoked modulation of activity. In the barrel cortex, the evoked activity of individual neurons therefore often falls dramatically outside the range of spontaneous activity (in contrast to [Luczak et al., 2009](#); [Figure S3D](#)). Our results further show that coding in barrel cortex, in particular, during performance of a somatosensation-dependent task, is not necessarily sparse ([Jadhav et al., 2009](#)).

Some neurons discriminated trial types nearly perfectly, in agreement with prior studies from behaving primates in which single neurons outperform the animal ([de Lafuente and Romo, 2005](#); [Hernandez et al., 2000](#); [Newsome et al., 1989](#); [Palmer et al., 2007](#)). Over half of all neurons did not discriminate above chance levels ([Figure 8A](#)). Discrimination performance depended on the overall spike rate of the neuron and on cortical layer ([Figure 8](#)). There is therefore a large heterogeneity in the amount of information individual barrel cortex neurons carry about the task. L4 and L5 contained the most discriminative neurons and the highest fractions of discriminative neurons ([Figure 8B](#)); a few L2/3 neurons also discriminated at high levels (up to 92% correct). Thus, while L4 and L5 discriminated best on average, L2/3 contained a sparse group of discriminative

neurons, which may be sufficient to drive behavior ([Huber et al., 2008](#)). The differences in discrimination ability across layers likely reflect the fact that neurons in different cortical layers correspond to distinct nodes in the cortical wiring diagram ([Thomson and Lamy, 2007](#)). Whether animals base sensory decisions on an average across all sensory neurons of a class or on only the most discriminative neurons is a long-standing and unresolved question ([Parker and Newsome, 1998](#)). Gain- and loss-of-function manipulations promise to shed light on this issue ([O’Connor et al., 2009](#)).

By combining in vivo population calcium imaging with post hoc immunohistochemistry, we found that a sparse population of highly discriminative neurons in L2/3 included non-GABAergic (presumably excitatory) neurons. However, GABAergic neurons may also discriminate. First, we identified relatively few GABAergic neurons in the in vivo population calcium imaging data ([Figure S9](#)). Second, the relationship between spiking activity and GCaMP3 fluorescence, important for interpreting the latter, has been measured for L2/3 pyramidal ([Tian et al., 2009](#)) but not GABAergic neurons. GABAergic neurons in barrel cortex L2/3 show high spike rates and behavior-dependent

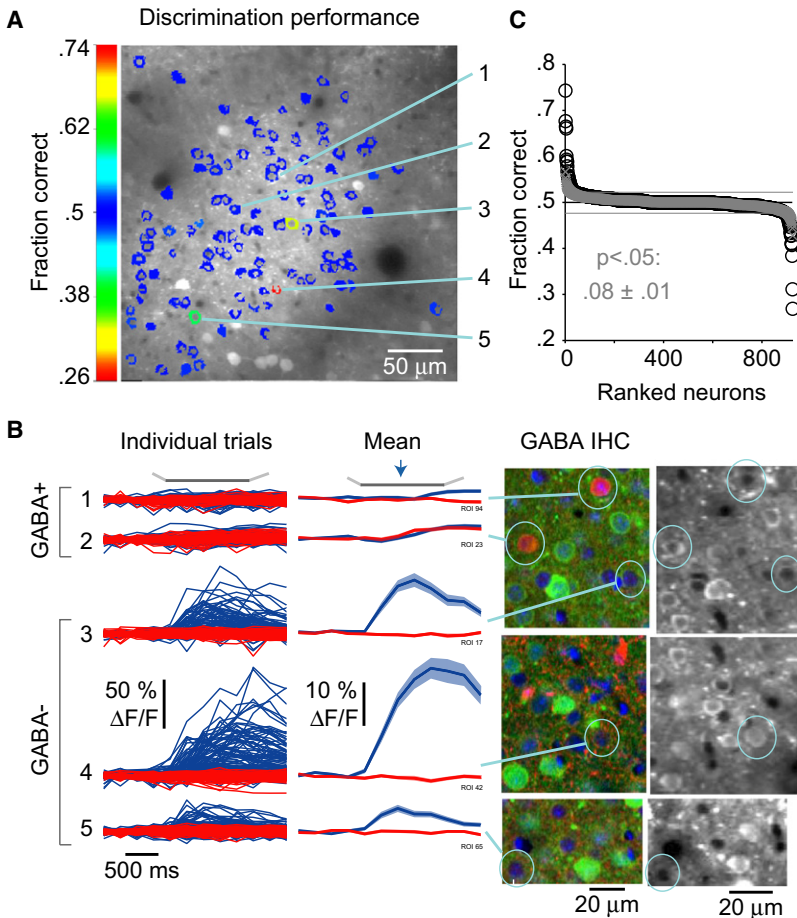


Figure 9. Discriminative Neurons Are Sparse in L2/3 and Include Excitatory Neurons

(A) Fraction of trials discriminated correctly (hits versus correct rejections) for multiple individual neurons from a mouse performing the localization task. Fraction correct is indicated for each neuron by the color scale. Colored pixels corresponding to each neuron are shown superimposed on a mean z-projection two-photon image from a single behavioral trial. Fraction correct is determined as the area under the receiver-operating characteristic (ROC) curve for a classifier based on event count, using only events in the first 2 s of the trial (see Experimental Procedures).

(B) Fluorescence ($\Delta F/F$) time series for individual hit (blue) and correct rejection (red) trials, and the corresponding means (\pm SEM), for two GABAergic (top two) and three non-GABAergic (bottom three) neurons. Confocal images (right) of the same neurons after immunohistochemistry for GABA and GFP (GCaMP3), and corresponding zoomed regions of the two-photon image shown in (A). Light gray slanted bar at top of traces indicates that the pole is in motion; dark gray horizontal bar indicates that the pole is at the end of its range and in reach of the whiskers. The blue arrow indicates the mean reaction time of the mouse during the recording.

(C) Black circles show fraction of trials discriminated correctly for multiple individual neurons from seven behavioral sessions from four mice. Gray crosses show fraction correct for each neuron after randomly shuffling the trial type labels (one instance of shuffling; for analyses the shuffling was repeated 100 times). Neurons are ranked by performance from best to worst along the x axis. The horizontal solid gray lines show the mean 2.5th and 97.5th percentiles from trial label-shuffled data. Data points between these lines show neurons that do not discriminate above chance level. Although the fraction of neurons falling outside the 2.5th and 97.5th percentiles of trial

label-shuffled (0.08 ± 0.01) data is similar to the expected fraction due to false positives (0.05), the distribution of neurons is clearly different from that of the label-shuffled data. For three mice, neurons were measured in two sessions and appear twice; there are 551 unique neurons. See also Figures S8 and S9.

modulations (Gentet et al., 2010). Although spike waveform measurements from our electrophysiological recordings did not yield clear clusters of putative fast- and regular-spiking neurons (Figure S1D), at least some discriminative neurons in L2/3 had high spike rates and narrow, symmetric spike waveforms (cf. Figures S1D and S4D). These discriminative neurons may have been fast-spiking interneurons (see also Hromadka et al., 2008).

Patterns of activity in barrel cortex during object localization were highly different for go and no-go trials. Mice appear to have tailored their whisking strategy to produce divergent interactions between whisker and pole (O'Connor et al., 2010) and therefore distinct patterns of activity in the barrel cortex. This active behavioral strategy focuses on the most relevant stimulus features, resulting in enhanced signal-to-noise in the underlying neural code.

In general, the fraction of discriminative neurons in barrel cortex is likely to depend on both the stimuli and on the behavioral relevance of the stimuli. For instance, if the mouse must make a choice based on the stimuli that determines whether it will be rewarded or punished (i.e., if the stimuli must be attended), the activity of a cortical neuron may be altered due to attention (Hubel

et al., 1959; Moran and Desimone, 1985) and neuromodulatory inputs (Metherate and Ashe, 1991; Svoboda et al., 1999). The simplicity of our task and the high level of motivation of the mice may have contributed to redundancy in coding. In tasks where stimuli do not need to be identified or localized (Jadhav et al., 2009), the activity patterns in somatosensory cortex resulting from different stimuli may be less well separated than in tasks requiring active discrimination (Krupa et al., 2004; von Heimendahl et al., 2007).

Finally, we found dramatic differences among cortical layers in overall spike rates and in the degree to which neurons of different layers carried information about the trial type. Neurons in L2/3, a major source of corticocortical output from the barrel cortex, showed sparse and low activity. Assuming that neurons in three to five barrel columns contribute to coding object location, we estimate that 2000–3000 spikes in L2/3 underlie coding for object location. This is well in excess of the \sim 300 spikes from L2/3 neurons required to drive behavior (Huber et al., 2008). In L5, another major source of corticocortical output, \sim 18,000 spikes are evoked during localization, even though animals can report short action potential trains from single L5 neurons (Houweling and Brecht, 2008). The cortical code for object

location (at least at distances well above threshold) is both redundant and strikingly different among different output cell classes.

EXPERIMENTAL PROCEDURES

Details of the behavioral task, apparatus, high-speed videography, and whisker tracking have been described elsewhere (O'Connor et al., 2010). See also Supplemental Experimental Procedures.

Mice

All mice used in this study were adult (>P60) C57BL/6CrJ males (Charles River) (three for electrophysiology, four for in vivo imaging). For approximately 10 days prior to training, and on days without behavioral testing, mice were limited to 1 ml/day of water. On days with behavioral sessions, mice generally obtained all water for the day during the session (approximately 1 ml). Food was available ad libitum. The weight and health of the mice were monitored daily. Mice were occasionally given supplemental water beyond their daily ration of 1 ml. All procedures were in accordance with protocols approved by the Janelia Farm Research Campus Institutional Animal Care and Use Committee.

Behavior Apparatus

The stimulus object was a 1/16 in diameter pole (stainless steel dowel pin, McMaster) coupled to a linear slider (Schneeberger) which moved the pole in the anterior-posterior dimension, driven by a stepper motor with sub-micrometer resolution (Zaber). This assembly was mounted on a pneumatic linear slider (Festo) that rapidly (~0.5 s) brought the stimulus into and out of reach of the whiskers. The pole moved along a trajectory that was at a lateral distance of 9.8 or 12 mm from the midline of the mouse. The apparatus was enclosed in a custom light-isolation box. Mice were monitored with an infrared-sensitive video camera (Super Circuits) using 940 nm illumination. Puffs of compressed air (typically 10 psi) for punishment were delivered through a small metal tube (~2.3 mm ID) pointed at the face from a distance of several centimeters, and were gated by a solenoid valve (Nresearch). The apparatus was controlled by an open-source software system (<http://brodylab.princeton.edu/bcontrol>; Z. Mainen, C. Brody, C. Cuihanu).

Mice were placed in an aluminum (32 mm ID) tube such that their heads extended out the front. A surgically implanted headpost was immobilized using a custom mount extending to the sides of the mice. Mice were thereby head-fixed in a natural crouching position with their whiskers free to move around the space surrounding their heads.

A custom acrylic "lickport" used to record licks and to deliver water rewards was placed within reach of the tongue (Figure 1A). Licks were recorded using a phototransistor. Water rewards were delivered by gravity into the lickport under solenoid valve control. To limit the time water remained at the lickport, and to prevent pooling, water was pumped out of the lickport using a peristaltic pump.

Behavioral Task

We describe here the behavioral task used in the electrophysiology experiments. For imaging experiments, details differed as specified in the Supplementary Experimental Procedures. Trial types (go or no-go) were chosen randomly, subject to the constraint that not more than three consecutive trials of the same type were allowed. The pole was positioned for the upcoming trial during the intertrial interval. Target and distracter positions were fixed and differed by 4.29 mm (go posterior, no-go anterior). The trial began with the pole descending (time of descent ~0.5 s) into reach of the whiskers. The mouse had until 2 s from the start of the pole descent to either lick ("go" response) or withhold a lick ("no-go" response). However, licks were only counted as responses if they occurred in the "answer period," a window that ended at 2 s and followed a 0.75 s "grace period" starting at the onset of the pole descent, during which licks had no consequences. Thus, mice had to either make a lick response within a 1.25 s window or withhold licking (as appropriate). After a no-go response the pole started ascending out of the whisker field exactly 2 s after starting its descent into the whisker field.

Correct no-go responses ("correct rejections") were not rewarded, and incorrect no-go responses ("misses") were not punished. Licks occurring within the answer period were recorded as go responses. Correct go responses ("hits") were rewarded with a drop of water (~8 μ l). The trial paused for 2 s to give the mouse time to drink. Incorrect go responses ("false alarms") triggered a 200 ms airpuff and the start of a "time-out" period in which the trial was paused for 5 s. If the mouse licked during this time-out, it received an identical airpuff and the time-out period was restarted. Each trial ended with the pole ascending (~0.75 s).

Electrophysiology

To implant the titanium headpost, mice were anesthetized with isoflurane (~2% by volume in O₂; SurgiVet, Smiths Medical). Mice were allowed at least 3 days to recover prior to water restriction. The headpost had a ~5.9 × 5.2 mm hole that allowed access to the skull over left barrel cortex and around which a dental acrylic bowl was shaped. This recording "well" was filled with Kwik-Cast silicone elastomer (World Precision Instruments) and covered with a thin layer of dental acrylic.

After training and intrinsic signal imaging, a craniotomy was made at the location of the left-hemisphere targeted (D4, D3, or D2) barrel column. The bone was thinned using a round-head FG one-fourth carbide dental bur (Henry Schein) with a pneumatic dental drill (Midwest Dental Corp). After the bone became thin enough that it would easily flake, a bent 28 gauge hypodermic needle was used to carefully remove a small piece (diameter ~100–200 μ m). The first pipette used for cell-attached recordings punctured the dura, which, presumably because of the small size of the craniotomy, adhered well to the surrounding skull.

Loose-seal cell-attached recordings were made using an Axopatch 200B amplifier (Molecular Devices), in the craniotomies targeted by intrinsic signal imaging. "Silent neurons" referred to in the text and figures are neurons with spontaneous spike rates <0.0083 Hz for which we did not collect behavioral trials. See Supplemental Experimental Procedures.

Two-Photon Calcium Imaging

The genetically encoded calcium indicator GCaMP3 (Tian et al., 2009) was expressed under the human *synapsin-1* promoter following infection with recombinant adenoassociated virus (serotype 2/1; produced by the University of Pennsylvania Gene Therapy Program Vector Core). Surgical conditions were as described above. A craniotomy (~2 mm in diameter) was made over left barrel cortex of P40–50 mice. The dura was left intact. Virus-containing solution was slowly injected (20 nl per site, four to eight sites per mouse; depth ~300 μ m) into the exposed cortex. The injection system comprised a pulled glass pipette (broken and beveled to ~25–30 μ m OD; Drummond Scientific, Wiretrol II Capillary Microdispenser) backfilled with mineral oil. A fitted plunger was inserted into the pipette and advanced to displace the contents using a hydraulic manipulator (Narashige, MO-10). Retraction of the plunger was used to load the pipette with virus. The injection pipette was positioned with a Sutter MP-285 manipulator. Following injection, the craniotomy was covered with a glass coverslip sealed in place with dental acrylic (Jet Repair Acrylic, Lang Dental Mfg.). A titanium headpost was attached to the skull with cyanoacrylate glue and dental acrylic to permit head fixation, as with mice prepared for cell-attached recordings.

Intrinsic signal imaging was used to localize C-row barrel columns. A region of interest for two-photon imaging was chosen based on the overlap of the localized C-row columns and GCaMP3 fluorescence. We were able to visualize barrels and confirm barrel column locations post hoc in histological sections stained with an anti-GFP antibody. Fifteen to twenty days after virus injection, mice began training on the localization task and concomitant two-photon imaging sessions. Sessions analyzed here occurred between days 35 and 45 postinfection.

The behavior apparatus was mounted under a custom two-photon microscope. GCaMP3 was excited at 1000 nm (typically 20–80 mW at the back aperture) with a Ti:Sapphire laser (Mai Tai, Spectra Physics) and imaged through a Nikon 16 \times , 0.8 NA objective. Emission light passed through a 565 DCXR dichroic (Chroma Technology) and a BGG22 filter (Chroma Technology) and was detected by a GaAsP photomultiplier tube (10770PB-40, Hamamatsu). Images (512 pixels [0.6 μ m/pixel] × 256 pixels [1.2 μ m/pixel]); were

acquired continuously at 4 Hz using ScanImage software (Iyer et al., 2009; Pologruto et al., 2003). Synchronization with the real-time behavior software occurred via pulses sent to ScanImage.

Electrophysiology Data Set and Analysis

The data set comprised 92 neurons recorded during task performance, plus 14 “silent neurons,” recorded in three craniotomies each (whisker barrel columns D2, D3, D4) in three mice (Figure S1E). Spike times were determined by finding local maxima above a threshold (Figure S1A) after high-pass filtering (Butterworth filter; 500 Hz cutoff). The threshold was adjusted for each trial and spike detection was confirmed. In many recordings, smaller amplitude spikes, presumably from nearby nonpatched neurons, were apparent. These secondary neurons were unambiguously separable from the patched cell by simple amplitude thresholding or the relevant trials were rejected from the analysis.

To estimate the depths of recorded neurons, we used the micromanipulator axial depth readings and subtracted 100 μm to account for estimated dimpling (Figure S1C). All depths reported in the text and figures are so adjusted. Laminar boundaries were considered to occur at 418 μm (L2/3 \rightarrow L4), 588 μm (L4 \rightarrow L5), and 890 μm (L5 \rightarrow L6) (Lefort et al., 2009).

PSTHs for display in figures were binned in 100 ms bins; error shading shows SEM. For all analyses using PSTHs the bin size was 50 ms.

Unless otherwise specified, and with the exception of “silent neurons,” all analyses include only data from periods in which the mouse was performing (Figure S1E).

Single-Neuron Discrimination Analyses

We quantified the discrimination performance of single neurons using a receiver-operating characteristic (ROC) analysis, with classification based on the similarity of each trial to the mean PSTHs for hit and correct rejection trials (Figure S6A).

Each trial was assigned a “decision variable” score (DV) equal to the dot-product similarity to the mean PSTH for hit trials minus the dot-product similarity to the mean PSTH for correct rejection trials. These mean PSTHs were calculated separately for each trial, with the current trial omitted from the mean PSTH for its trial type. That is, $DV = t_i (\overline{H}_{v_j \neq i} - \overline{CR})$ for hit trials and $DV = t_i (\overline{H} - \overline{CR}_{v_j \neq i})$ for correct rejection trials, where t_i is the single-trial PSTH for the i -th trial, \overline{H} and \overline{CR} are the mean hit and correct rejection PSTHs. Larger DV imply greater similarity to the mean hit PSTH compared with the mean correct rejection PSTH. An observer (classifier) could assign individual trials as either a hit or a correct rejection based on whether the value of this decision variable for a given trial was greater or less than a criterion value ($DV > \text{crit}$: “hit,” else: “correct rejection;” Figure S6A). To determine what fraction of trials an ideal observer could classify correctly based on this decision variable, an ROC curve (Green and Swets, 1966) was constructed. The ROC curve was obtained by varying the criterion across DV. At each criterion value, the probability that a correct rejection trial exceeded the criterion value was plotted (on the x axis) against the probability that a hit trial exceeded the criterion (on the y axis; Figure S6A). The area under the ROC curve (AUC) is equivalent to the fraction of trials that would be decided correctly by an ideal observer making decisions based on DV (Green and Swets, 1966). We used AUC as the measure of single-neuron performance (“fraction correct” in Figures 8, S4, S6B, and S7). Fraction correct for individual neurons as a function of time from the start of the trial, T (Figures 8E and S7B), was computed as the area under the ROC curve using all PSTH bins with bin centers at times $t \leq T$.

For analyses of spiking activity “prior to the reaction time,” only PSTH bins up to and including the bin containing the mean reaction time for each recording were included. For analyses of spiking activity over the “full trial,” all PSTH bins covering 5 s from the start of each trial were used.

Calcium Imaging Data Analysis

Data from four mice in seven total sessions were analyzed. Regions of interest (ROIs) corresponding to individual neurons were defined by manually outlining an ROI border and then semiautomatically selecting pixels that were part of the neuron. Since GCaMP3 generally fills the cytosol and not the nucleus (Tian et al., 2009), it was important to omit the nucleus from the ROI. In mice where multiple sessions were used, a normalized cross-correlation algorithm using

small rectangular subregions around the ROI as target images was employed to align ROIs across sessions.

For each neuron, $\Delta F/F$ was calculated as $(F - F_0) / F_0$, where F is the time series of raw fluorescence averaged over all the neuron’s pixels and F_0 is the mode of a kernel density estimate (MATLAB R2008b “ksdensity” function) of F within a moving window of 55 s. For traces shown in Figures 9 and S8 only, F_0 was the mean of F over the first four frames of each trial.

Transient increases in $\Delta F/F$ (“events”) were detected using a simple threshold-based method similar to published methods (Dombeck et al., 2007, 2009).

We adapted the single-neuron discrimination analysis used for the cell-attached recordings to the fluorescence data (Figures 9 and S8). Because of the limited temporal resolution of the imaging data, we used a method based on event count rather than the full time-varying modulation pattern used in the ideal-observer analysis of electrophysiology data (Figure 8). This adaptation is equivalent to the spike count version of the ideal-observer analysis (Figure S7C) described above, but with events substituted for spikes. We considered only those events occurring in the first 2 s of the trial, corresponding to the frame before the mice typically started licking to indicate a go response (because in the imaging experiments mice received a reward only after a delay, the precise reaction time was difficult to quantify). Because of limited temporal resolution of the calcium indicator, typically either zero or one event occurred in this period.

SUPPLEMENTAL INFORMATION

Supplemental Information includes Supplemental Experimental Procedures and figures and can be found with this article online at doi:10.1016/j.neuron.2010.08.026.

ACKNOWLEDGMENTS

This work was funded by the Howard Hughes Medical Institute. We thank Nathan Clack and Gene Myers for whisker tracking software; Jinyang Liu and Tim O’Connor for programming; Lin Tian and Loren Looger for GCaMP3 virus; Dan Flickinger for mechanical design; Nick Betley, Amy Hu, Brenda Shields, Boris Zemelman, Tomáš Hromádka and Tony Zador for advice; Andrew Hires, Tomáš Hromádka and Miguel Maravall for comments on the manuscript.

Accepted: August 5, 2010

Published: September 22, 2010

REFERENCES

- Adrian, E. (1932). *The Mechanisms of Nervous Action* (Philadelphia: University of Pennsylvania Press).
- Andermann, M.L., Kerlin, A.M., and Reid, R.C. (2010). Chronic cellular imaging of mouse visual cortex during operant behavior and passive viewing. *Front Cell Neurosci* 4, 3.
- Armstrong-James, M., Fox, K., and Das-Gupta, A. (1992). Flow of excitation within rat barrel cortex on striking a single vibrissa. *J. Neurosci.* 68, 1345–1358.
- Barlow, H.B. (1953). Action potentials from the frog’s retina. *J. Physiol.* 119, 58–68.
- Birdwell, J.A., Solomon, J.H., Thajchayapong, M., Taylor, M.A., Cheely, M., Towal, R.B., Conradt, J., and Hartmann, M.J. (2007). Biomechanical models for radial distance determination by the rat vibrissal system. *J. Neurophysiol.* 98, 2439–2455.
- Brecht, M., and Sakmann, B. (2002). Dynamic representation of whisker deflection by synaptic potentials in spiny stellate and pyramidal cells in the barrels and septa of layer 4 rat somatosensory cortex. *J. Physiol.* 543, 49–70.
- Brecht, M., Roth, A., and Sakmann, B. (2003). Dynamic receptive fields of reconstructed pyramidal cells in layers 3 and 2 of rat somatosensory barrel cortex. *J. Physiol.* 553, 243–265.

- Britten, K.H., Shadlen, M.N., Newsome, W.T., and Movshon, J.A. (1992). The analysis of visual motion: a comparison of neuronal and psychophysical performance. *J. Neurosci.* *12*, 4745–4765.
- Buzsáki, G. (2004). Large-scale recording of neuronal ensembles. *Nat. Neurosci.* *7*, 446–451.
- Celebrini, S., and Newsome, W.T. (1994). Neuronal and psychophysical sensitivity to motion signals in extrastriate area MST of the macaque monkey. *J. Neurosci.* *14*, 4109–4124.
- Cohen, M.R., and Newsome, W.T. (2009). Estimates of the contribution of single neurons to perception depend on timescale and noise correlation. *J. Neurosci.* *29*, 6635–6648.
- Cook, E.P., and Maunsell, J.H. (2002). Dynamics of neuronal responses in macaque MT and VIP during motion detection. *Nat. Neurosci.* *5*, 985–994.
- Crochet, S., and Petersen, C.C. (2006). Correlating whisker behavior with membrane potential in barrel cortex of awake mice. *Nat. Neurosci.* *9*, 608–610.
- Croner, L.J., and Albright, T.D. (1999). Segmentation by color influences responses of motion-sensitive neurons in the cortical middle temporal visual area. *J. Neurosci.* *19*, 3935–3951.
- Curtis, J.C., and Kleinfeld, D. (2009). Phase-to-rate transformations encode touch in cortical neurons of a scanning sensorimotor system. *Nat. Neurosci.* *12*, 492–501.
- de Kock, C.P., Bruno, R.M., Spors, H., and Sakmann, B. (2007). Layer- and cell-type-specific suprathreshold stimulus representation in rat primary somatosensory cortex. *J. Physiol.* *581*, 139–154.
- de Kock, C.P., and Sakmann, B. (2008). High frequency action potential bursts (>or= 100 Hz) in L2/3 and L5B thick tufted neurons in anaesthetized and awake rat primary somatosensory cortex. *J. Physiol.* *586*, 3353–3364.
- de Kock, C.P.J., and Sakmann, B. (2009). Spiking in primary somatosensory cortex during natural whisking in awake head-restrained rats is cell-type specific. *Proc. Natl. Acad. Sci. USA* *106*, 16446–16450.
- de Lafuente, V., and Romo, R. (2005). Neuronal correlates of subjective sensory experience. *Nat. Neurosci.* *8*, 1698–1703.
- DeWeese, M.R., Wehr, M., and Zador, A.M. (2003). Binary spiking in auditory cortex. *J. Neurosci.* *23*, 7940–7949.
- Diamond, M.E., von Heimendahl, M., Knutsen, P.M., Kleinfeld, D., and Ahissar, E. (2008). “Where” and “what” in the whisker sensorimotor system. *Nat. Rev. Neurosci.* *9*, 601–612.
- Dombeck, D.A., Khabbazi, A.N., Collman, F., Adelman, T.L., and Tank, D.W. (2007). Imaging large-scale neural activity with cellular resolution in awake, mobile mice. *Neuron* *56*, 43–57.
- Dombeck, D.A., Graziano, M.S., and Tank, D.W. (2009). Functional clustering of neurons in motor cortex determined by cellular resolution imaging in awake behaving mice. *J. Neurosci.* *29*, 13751–13760.
- Fox, K. (2002). Anatomical pathways and molecular mechanisms for plasticity in the barrel cortex. *Neuroscience* *111*, 799–814.
- Gentet, L.J., Avermann, M., Matyas, F., Staiger, J.F., and Petersen, C.C. (2010). Membrane potential dynamics of GABAergic neurons in the barrel cortex of behaving mice. *Neuron* *65*, 422–435.
- Green, D.M., and Swets, J.A. (1966). *Signal detection theory and psychophysics* (New York: Wiley).
- Greenberg, D.S., Houweling, A.R., and Kerr, J.N. (2008). Population imaging of ongoing neuronal activity in the visual cortex of awake rats. *Nat. Neurosci.* *11*, 749–751.
- Helmchen, F., and Denk, W. (2005). Deep tissue two-photon microscopy. *Nat. Methods* *2*, 932–940.
- Helmchen, F., Svoboda, K., Denk, W., and Tank, D.W. (1999). In vivo dendritic calcium dynamics in deep-layer cortical pyramidal neurons. *Nat. Neurosci.* *2*, 989–996.
- Hernandez, A., Zainos, A., and Romo, R. (2000). Neuronal correlates of sensory discrimination in the somatosensory cortex. *Proc. Natl. Acad. Sci. USA* *97*, 6191–6196.
- Houweling, A.R., and Brecht, M. (2008). Behavioural report of single neuron stimulation in somatosensory cortex. *Nature* *451*, 65–68.
- Hromádka, T., Deweese, M.R., and Zador, A.M. (2008). Sparse representation of sounds in the unanesthetized auditory cortex. *PLoS Biol.* *6*, e16.
- Hubel, D.H. (1957). Tungsten Microelectrode for Recording from Single Units. *Science* *125*, 549–550.
- Hubel, D.H., and Wiesel, T.N. (1962). Receptive fields, binocular interaction and functional architecture in the cat’s visual cortex. *J. Physiol.* *160*, 106–154.
- Hubel, D.H., Henson, C.O., Rupert, A., and Galambos, R. (1959). Attention units in the auditory cortex. *Science* *129*, 1279–1280.
- Huber, D., Petreanu, L., Ghilani, N., Ranade, S., Hromádka, T., Mainen, Z., and Svoboda, K. (2008). Sparse optical microstimulation in barrel cortex drives learned behaviour in freely moving mice. *Nature* *451*, 61–64.
- Iyer, V., O’Connor, T., Chiappe, E., Huber, D., Petreanu, L., Jayaraman, V., Shepherd, G.M., and Svoboda, K. (2009). ScanImage for in vivo laser scanning microscopy Program No. 485.2. 2009 Neuroscience Meeting Planner. Chicago, IL: Society for Neuroscience. Online.
- Jadhav, S.P., Wolfe, J., and Feldman, D.E. (2009). Sparse temporal coding of elementary tactile features during active whisker sensation. *Nat. Neurosci.* *12*, 792–800.
- Kerr, J.N., de Kock, C.P., Greenberg, D.S., Bruno, R.M., Sakmann, B., and Helmchen, F. (2007). Spatial organization of neuronal population responses in layer 2/3 of rat barrel cortex. *J. Neurosci.* *27*, 13316–13328.
- Kleinfeld, D., Ahissar, E., and Diamond, M.E. (2006). Active sensation: insights from the rodent vibrissa sensorimotor system. *Curr. Opin. Neurobiol.* *16*, 435–444.
- Komiyama, T., Sato, T.R., O’Connor, D.H., Zhang, Y.X., Huber, D., Hooks, B.M., Gabbito, M., and Svoboda, K. (2010). Learning-related fine-scale specificity imaged in motor cortex circuits of behaving mice. *Nature* *464*, 1182–1186.
- Krupa, D.J., Wiest, M.C., Shuler, M.G., Laubach, M., and Nicolelis, M.A. (2004). Layer-specific somatosensory cortical activation during active tactile discrimination. *Science* *304*, 1989–1992.
- Lefort, S., Tomm, C., Floyd Sarria, J.C., and Petersen, C.C. (2009). The excitatory neuronal network of the C2 barrel column in mouse primary somatosensory cortex. *Neuron* *61*, 301–316.
- Luczak, A., Bartho, P., and Harris, K.D. (2009). Spontaneous events outline the realm of possible sensory responses in neocortical populations. *Neuron* *62*, 413–425.
- Manns, I.D., Sakmann, B., and Brecht, M. (2004). Sub- and suprathreshold receptive field properties of pyramidal neurones in layers 5A and 5B of rat somatosensory barrel cortex. *J. Physiol.* *556*, 601–622.
- Margrie, T.W., Brecht, M., and Sakmann, B. (2002). In vivo, low-resistance, whole-cell recordings from neurons in the anaesthetized and awake mammalian brain. *Pflügers Arch.* *444*, 491–498.
- Metherate, R., and Ashe, J.H. (1991). Basal forebrain stimulation modifies auditory cortex responsiveness by an action at muscarinic receptors. *Brain Res.* *559*, 163–167.
- Mitchinson, B., Martin, C.J., Grant, R.A., and Prescott, T.J. (2007). Feedback control in active sensing: rat exploratory whisking is modulated by environmental contact. *Proc. Biol. Sci.* *274*, 1035–1041.
- Moore, C.I., and Nelson, S.B. (1998). Spatio-temporal subthreshold receptive fields in the vibrissa representation of rat primary somatosensory cortex. *J. Neurophysiol.* *80*, 2882–2892.
- Moran, J., and Desimone, R. (1985). Selective attention gates visual processing in the extrastriate cortex. *Science* *229*, 782–784.
- Mountcastle, V.B. (1995). The parietal system and some higher brain functions. *Cereb. Cortex* *5*, 377–390.
- Newsome, W.T., Britten, K.H., and Movshon, J.A. (1989). Neuronal correlates of a perceptual decision. *Nature* *341*, 52–54.
- O’Connor, D.H., Huber, D., and Svoboda, K. (2009). Reverse engineering the mouse brain. *Nature* *461*, 923–929.

- O'Connor, D.H., Clack, N.G., Huber, D., Komiyama, T., Myers, E.W., and Svoboda, K. (2010). Vibrissa-based object localization in head-fixed mice. *J. Neurosci.* *30*, 1947–1967.
- Olshausen, B.A., and Field, D.J. (2004). Sparse coding of sensory inputs. *Curr. Opin. Neurobiol.* *14*, 481–487.
- Otazu, G.H., Tai, L.H., Yang, Y., and Zador, A.M. (2009). Engaging in an auditory task suppresses responses in auditory cortex. *Nat. Neurosci.* *12*, 646–654.
- Palmer, C., Cheng, S.Y., and Seidemann, E. (2007). Linking neuronal and behavioral performance in a reaction-time visual detection task. *J. Neurosci.* *27*, 8122–8137.
- Pantoja, J., Ribeiro, S., Wiest, M., Soares, E., Gervasoni, D., Lemos, N.A., and Nicolelis, M.A. (2007). Neuronal activity in the primary somatosensory thalamo-cortical loop is modulated by reward contingency during tactile discrimination. *J. Neurosci.* *27*, 10608–10620.
- Parker, A.J., and Newsome, W.T. (1998). Sense and the single neuron: probing the physiology of perception. *Annu. Rev. Neurosci.* *21*, 227–277.
- Petersen, C.C. (2007). The functional organization of the barrel cortex. *Neuron* *56*, 339–355.
- Pologruto, T.A., Sabatini, B.L., and Svoboda, K. (2003). ScanImage: Flexible software for operating laser-scanning microscopes. *Biomed. Eng. Online* *2*, 13.
- Poulet, J.F., and Petersen, C.C. (2008). Internal brain state regulates membrane potential synchrony in barrel cortex of behaving mice. *Nature* *454*, 881–885.
- Prince, S.J., Pointon, A.D., Cumming, B.G., and Parker, A.J. (2000). The precision of single neuron responses in cortical area V1 during stereoscopic depth judgments. *J. Neurosci.* *20*, 3387–3400.
- Romo, R., Hernandez, A., Zainos, A., and Salinas, E. (1998). Somatosensory discrimination based on cortical microstimulation. *Nature* *392*, 387–390.
- Sato, T.R., Gray, N.W., Mainen, Z.F., and Svoboda, K. (2007). The functional microarchitecture of the mouse barrel cortex. *PLoS Biol.* *5*, e189.
- Shadlen, M.N., and Newsome, W.T. (1994). Noise, neural codes and cortical organization. *Curr. Opin. Neurobiol.* *4*, 569–579.
- Shadlen, M.N., and Newsome, W.T. (1998). The variable discharge of cortical neurons: implications for connectivity, computation, and information coding. *J. Neurosci.* *18*, 3870–3896.
- Shoham, S., O'Connor, D.H., and Segev, R. (2006). How silent is the brain: is there a “dark matter” problem in neuroscience? *J. Comp. Physiol. A Neuroethol. Sens. Neural Behav. Physiol.* *192*, 777–784.
- Simons, D.J. (1978). Response properties of vibrissa units in rat SI somatosensory neocortex. *J. Neurophysiol.* *41*, 798–820.
- Simons, D.J., Carvell, G.E., Hershey, A.E., and Bryant, D.P. (1992). Responses of barrel cortex neurons in awake rats and effects of urethane anesthesia. *Exp. Brain Res.* *91*, 259–272.
- Stosiek, C., Garaschuk, O., Holthoff, K., and Konnerth, A. (2003). In vivo two-photon calcium imaging of neuronal networks. *Proc. Natl. Acad. Sci. USA* *100*, 7319–7324.
- Svoboda, K., and Yasuda, R. (2006). Principles of two-photon excitation microscopy and its applications to neuroscience. *Neuron* *50*, 823–839.
- Svoboda, K., Denk, W., Kleinfeld, D., and Tank, D.W. (1997). In vivo dendritic calcium dynamics in neocortical pyramidal neurons. *Nature* *385*, 161–165.
- Svoboda, K., Helmchen, F., Denk, W., and Tank, D.W. (1999). The spread of dendritic excitation in layer 2/3 pyramidal neurons in rat barrel cortex *in vivo*. *Nat. Neurosci.* *2*, 65–73.
- Thomson, A.M., and Lamy, C. (2007). Functional maps of neocortical local circuitry. *Front Neurosci* *1*, 19–42.
- Tian, L., Hires, S.A., Mao, T., Huber, D., Chiappe, M.E., Chalasani, S.H., Petreanu, L., Akerboom, J., McKinney, S.A., Schreiter, E.R., et al. (2009). Imaging neural activity in worms, flies and mice with improved GCaMP calcium indicators. *Nat. Methods* *6*, 875–881.
- Tsai, P.S., Kauffhold, J.P., Blinder, P., Friedman, B., Drew, P.J., Karten, H.J., Lyden, P.D., and Kleinfeld, D. (2009). Correlations of neuronal and microvascular densities in murine cortex revealed by direct counting and colocalization of nuclei and vessels. *J. Neurosci.* *29*, 14553–14570.
- Uka, T., and DeAngelis, G.C. (2003). Contribution of middle temporal area to coarse depth discrimination: comparison of neuronal and psychophysical sensitivity. *J. Neurosci.* *23*, 3515–3530.
- Vijayan, S., Hale, G.J., Moore, C.I., Brown, E.N., and Wilson, M.A. (2010). Activity in the barrel cortex during active behavior and sleep. *J. Neurophysiol.* *103*, 2074–2084.
- von Heimendahl, M., Itskov, P.M., Arabzadeh, E., and Diamond, M.E. (2007). Neuronal activity in rat barrel cortex underlying texture discrimination. *PLoS Biol.* *5*, e305.
- Welker, C. (1971). Microelectrode delineation of fine grain somatotopic organization of (Sml) cerebral neocortex in albino rat. *Brain Res.* *26*, 259–275.
- Woolsey, T.A., and Van der Loos, H. (1970). The structural organization of layer IV in the somatosensory region (SI) of mouse cerebral cortex. The description of a cortical field composed of discrete cytoarchitectonic units. *Brain Res.* *17*, 205–242.
- Wurtz, R.H. (1968). Visual cortex neurons: response to stimuli during rapid eye movements. *Science* *162*, 1148–1150.